J. Fluid Mech. (1983), *vol.* 129, *pp.* 1–25
Printed in Great Britain

Turbulent bores and hydraulic jumps

By P. A. MADSEN† AND I. A. SVENDSEN

Institute of Hydrodynamics and Hydraulic Engineering (ISVA), Technical University of Denmark, Building 115, DK 2800 Lyngby, Denmark

(Received 22 February 1982 and in revised form 13 August 1982)

A theoretical model for the velocity field and the surface profile of bores and hydraulic jumps is developed. The turbulence is assumed to be concentrated in a wedge that originates at the toe of the front and spreads towards the bottom, and the turbulent closure used is a simplified k-ϵ model allowing for non-equilibrium in the turbulent kinetic energy. The flow equations are satisfied in depth-integrated form (method of weighted residuals), and measured deviations from static pressure are analysed and shown to have a negligible effect on the results. Comparison with measurements shows good agreement, but there is a clear need for further experimental results in the highly turbulent region near the free surface. Some basic mechanisms of the flow are discussed and explained from the theory.

1. Introduction

Bores and hydraulic jumps are nearly equivalent flows. The jump is a stationary transition to subcritical flow that may occur in a supercritical stream, and a bore is a transition to a higher water level propagating into quiescent water of a lower level.

The difference between a bore and a hydraulic jump lies in the bottom boundary layer generated in the latter case owing to the flowing water. In a bore a much weaker bottom boundary layer is initiated at the front, and it will not be significant until far behind the bore and well outside the region in which we are interested.

We shall consider these two flows together since we intend to neglect the bottom boundary layer and concentrate on the violent turbulence in the front and near the surface and its effect on the flow pattern. This assumption will be justified. Hence in our considerations a bore may be turned into a hydraulic jump by watching it from a coordinate system moving with the bore.

The purpose of the present paper is to develop a theoretical model for such bores and jumps using a simple turbulence model to describe the flow, the shear stresses and the energy dissipation in the flow.

Our interest in these flows stems from the observation that the front of a periodic wave in the surf zone has many features in common with the steady bore/hydraulic jump.

In the literature, studies of the propagating bores are usually made by idealizing the bore to a moving discontinuity. Then the surrounding flow is described by the nonlinear shallow-water equations (see e.g. Peregrine 1972; Svendsen & Jonsson 1976), which are studied either by the method of characteristics (as e.g. Peregrine 1974) or numerically (as e.g. by Hibberd & Peregrine 1979) or by approximate methods (Keller, Levine & Whitham 1969). In this type of model, however, the shape of the front and the flow beneath it are not described at all.

† Present address: Danish Hydraulic Institute, Horsholm, Denmark.

Previous works on the detailed flow patterns in a hydraulic jump have (with a few exceptions) all been experimental, and a considerable number of investigations have been published with measurements of surface profiles, mean velocities and turbulence characteristics.

For a detailed survey of investigations up to 1967 we refer to Rajaratnam (1967). It may be mentioned that one of the first examples was Bakhmeteff & Matzke (1936), who, in addition to a discussion of the overall flow characteristics such as height (Bélanger 1828) and energy dissipation for a given Froude number

$$F_1 = u_1(gd_1)^{-\frac{1}{2}}, \tag{1.1}$$

also presented measurements of the surface profile which will be used for comparisons in §6.

Measurements of surface profiles have also been reported by Rouse, Siao & Nagaratnam (1958), who measured velocities in a wind tunnel in which they modelled the jump by replacing the free surface by a solid wall shaped according to measurements in a hydraulic flume.

Velocity measurements were also made by Resch & Leutheusser (1972*a*, *b*) and by Resch, Leutheusser & Coantic (1976). These publications (as well as Rouse *et al.* 1958) included data and discussions of various turbulent flow quantities such as $\overline{u'^2}$, $\overline{w'^2}$ *and* $\overline{u'w'}$.

Lately Battjes & Sakai (1981) have presented velocity measurements in a bore-like flow generated behind an airfoil suspended in flowing water. Their results, however, are not directly comparable with the flow beneath a hydraulic jump because of the large depth of water beneath the airfoil.

A few contributions suggest theoretical models for the flow in a hydraulic jump.

Both Rajaratnam (1965) and Narayanan (1975) suggested that the turbulent flow in a jump resembles that in a wall jet. A theoretical approach based on the wall jet analogy was given by Narayanan. He assumed one type similarity in the bottom boundary layer and another type in the outer layer. The pressure was assumed hydrostatic and the shear stresses were described by empirical expressions known from wall jets and shear layers respectively. The set-up used, however, resulted in a discontinuity in the free surface.

A different model was analysed by Tsubaki (1950). He assumed, however, that the turbulence was limited to a region above the level of the upstream free surface (figure 1*b*). As shown by Peregrine & Svendsen (1978) this does not hold. The turbulence continues to spread downwards from its initiation at the toe of the front until it reaches the bottom somewhere downstream of the jump (figure 1*c*).

This observation also differs from the assumptions made by Longuet-Higgins & Turner (1974). They considered the front of breaking waves and assumed that the turbulence was limited to the region with air entrainment (figure 1*a*).

Finally Johns (1980) considered periodic and single bores on a sloping bottom. The pressure was assumed to be hydrostatic, and the non-stationary differential equations of mass, horizontal momentum, and turbulent kinetic energy were solved numerically. The model allowed for a non-equilibrium state in turbulent kinetic energy k, but included no generation of surface turbulence, and, in consequence, the resulting velocity distribution turned out to be nearly uniform over the depth, obviously dominated by the bottom rather than by the free shear flow.

Thus, in spite of the general impression that the hydraulic jump is a well-studied flow phenomenon, no proper theoretical model is available for the flow field.

The present paper will describe a theory based on the observations described by

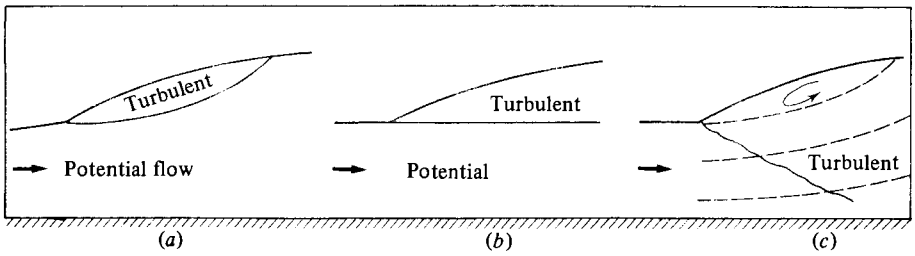

FIGURE 1. The extension of the shear flow in a bore: (*a*) Longuet-Higgins & Turner (1974); (*b*) Tsubaki (1950); (*c*) present model.

Peregrine & Svendsen (1978). The basic assumptions will be presented and discussed in §2, and throughout the presentation emphasis will be given to justifying the various simplifications and illustrating the sensitivity of the result to deviations from the conditions assumed. One assumption is to neglect deviations from static pressure (it is shown why this is acceptable), and we also assume a longitudinal lengthscale much longer than the vertical lengthscale. The resulting problem will resemble a boundary-layer problem with a pressure gradient. The conditions required for similarity solutions to such a problem are not satisfied (Falkner & Scan 1930) even for the (rather unrealistic) model based on a constant eddy viscosity. And Madsen (1981) showed that a more realistic turbulence model cannot change this conclusion.

Instead the flow pattern is determined by the method of weighted residuals, which implies that the basic equations are integrated over part of the water depth and satisfied at large. This is a generalization of the method that von Kármán (1930) showed yields accurate results for the boundary layer over a flat plate.

The depth-integrated equations and the solution for the velocity profiles are presented in §3, and in §4 we discuss the turbulent closure and analyse some properties of the velocity field. It is shown how the flow model suggested can account for the effect of the free-surface turbulence in the roller and the non-equilibrium state of turbulent kinetic energy.

In §5 the free-surface profile is determined, and in §6 the surface profile and the velocities and shear stresses derived from the theory are compared with measurements. The agreement is shown to be quite satisfactory and deviations as well as discrepancies in the measurements available are analysed.

Some important details of the flow are investigated further in §7, and the discussion in this section as well as in §8 includes a critical evaluation of the results. The conclusions are summarized in §8.

There are three appendices describing in more detail some essential points in the main text.

2. Preliminary considerations

It is useful first to discuss the characteristics of the flow with the purpose in mind of introducing suitable assumptions.

First we notice that, although Rajaratnam (1965) showed experimentally that the pressure variation is not static, the deviation will have a very small effect on the horizontal momentum balance (see appendix A). Hence we adopt the assumption of static pressure, by which we also exclude the possibility of describing undular bores, that is we assume that $F_1^2 \gtrsim 2$.

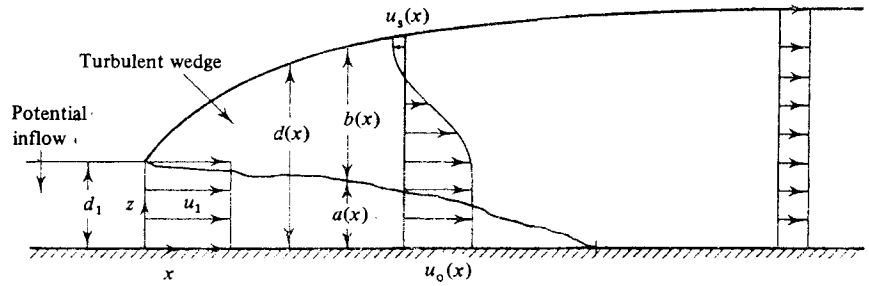

FIGURE 2. Definitions related to the flow considered.

In close agreement with the actual flow pattern we shall also assume that the horizontal lengthscale for the flow is much larger than the vertical scale. This does not change the continuity equation, which reads

$$\frac{\partial \bar{u}}{\partial x}+\frac{\partial \bar{w}}{\partial z}=0, \tag{2.1}$$

but the Reynolds equations governing general turbulent flow degenerate into the form

$$\bar{u}\frac{\partial \bar{u}}{\partial x}+\bar{w}\frac{\partial \bar{u}}{\partial z}=-\frac{1}{\rho}\frac{\partial \bar{p}}{\partial x}+\frac{\partial}{\partial z}(-\overline{u'w'}) \tag{2.2}$$

(see figure 2 for definitions). Here

$$u=\bar{u}+u', \quad w=\bar{w}+w' \tag{2.3}$$

are horizontal and vertical velocity components respectively, the overbar denoting ensemble-averaging and the prime representing turbulent fluctuations. This implies that the flow we consider (like a number of other turbulent shear flows such as mixing layers, wakes and various types of jets) is described by the boundary-layer equations with a pressure gradient.

Some of the flows mentioned (viz. mixing layers, free or strong jets) have similarity solutions (see e.g. Rajaratnam 1976; Abramovich 1963), which for the present problem would be described by the fairly general expression

$$\left.\begin{aligned} \bar{u}(x,z) &= u_0(x)\,(1+\Gamma(x)f(\sigma)) \quad (0\leqslant\sigma\leqslant 1), \\ \sigma &= \frac{z-a(x)}{b(x)}, \end{aligned}\right\} \tag{2.4}$$

which has the four parameters u_0, Γ, a and b.

Here $u_0(x)$ is the (horizontal) velocity outside the turbulent region, b is the height of that region, and $z-a$ is the vertical height above its lower edge.

Such solutions, however, exist only for certain types of flow (Falkner & Scan 1930) which are not satisfied in the present case (Madsen 1981). Thus we cannot expect an expression of the type (2.4) to satisfy the equations of motion in all detail.

Instead of seeking such solutions we choose to satisfy the equations 'at large' by using an integral method which consists of specifying a suitable form of $f(\sigma)$ and require that the depth-integrated versions of (2.1) and (2.2) are satisfied for all x.†

† This method was first introduced by von Kármán (1930) for boundary-layer problems and has in more general form become known as the 'method of weighted residuals' (see e.g. Finlayson 1972). For the boundary-layer type of problems it is known to yield results with x-variations that are remarkably insensitive to inaccuracies in the z-variations prescribed for the velocity profile $\bar{u}(x,z)$.

In other words, total mass and momentum are conserved, and if our conjecture for the velocity variation with z (i.e. $f(\sigma)$) is reasonable, many details will also be correctly reproduced.

The physical assumptions used on the velocity profile in the turbulent region is that at the lower edge ($z = a$) we must have the same velocity as in the non-turbulent flow, and at the same time the turbulent shear stresses τ_{zx} must vanish. Thus we use

$$u = u_0(x), \quad \frac{\partial u}{\partial z} = 0 \quad \text{at} \quad z = a(x), \tag{2.5a}$$

and add

$$u = u_s(x) \quad \text{at} \quad z = d(x). \tag{2.5b}$$

This essentially introduces u_0 and u_s as two of the variables of the problem. Substituting this into (2.4) yields

$$\Gamma(x) = \frac{u_s}{u_0} - 1. \tag{2.6}$$

For $f(\sigma)$ a third-order polynomial is used. When (2.5) is invoked this takes the form

$$f(\sigma) = -A\sigma^3 + (1+A)\sigma^2 \quad (0 < \sigma < 1), \tag{2.7}$$

with

$$f(0) = 0, \quad f(1) = 1.$$

The justification for this choice and the value of A will be discussed further in connection with the turbulent closure (§4).

Outside the turbulent region we shall in this presentation only consider situations for which the velocity can be considered constant over the depth. This applies to the flow in front of the jump (which hence becomes of the type denoted 'undeveloped inflow' by Resch *et al.* 1976) as well as to the region beneath the turbulent zone in the front part of the jump.

Hence the bottom boundary layer and the associated bed shear stresses are neglected. These shear stresses will influence the height of the jump, particularly for large Froude numbers (see Harleman 1958). However, for $F = 8$, say, the effect is only about 4% on the height and inside the jump the effect will be even less as it accumulates downstream.

Thus the flow pattern we consider has a core (see figure 1) with depth-independent velocities that decrease downstream due to the increasing pressure.

The complete velocity profiles prescribed are given by

$$u(x,z) = \left\{ \begin{array}{ll} u_0(x) & (0 < z < a), \\ \text{see (2.4)} & (a < z < d). \end{array} \right\} \tag{2.8}$$

3. The integrated equations

The assumptions introduced above correspond to a problem that contains four unknown quantities, for which it is convenient to choose the velocity $u_s(x)$ at the mean free surface, the velocity $u_0(x)$ in the potential core, the thickness $a(x)$ of that layer, and the total depth $d(x)$.

Hence we can satisfy four integrated versions of the basic equations. One must be the continuity equation, which can be written

$$\frac{\partial}{\partial x}\int_0^d \bar{u}\, dz = 0. \tag{3.1}$$

We further choose to satisfy the equation of horizontal momentum integrated over the total depth and over the core region separately (which implies that horizontal momentum is also satisfied in the turbulent region separately).

Invoking the assumptions introduced in §2 the two momentum equations may be written

$$\frac{\partial}{\partial x}\left\{\int_0^d \bar{u}^2\,dz+\tfrac{1}{2}gd^2\right\}=0 \quad \text{total depth,} \tag{3.2}$$

$$\frac{\partial}{\partial x}\left\{\tfrac{1}{2}u_0^2+gd\right\}=0 \quad \text{for} \quad a\neq 0, \tag{3.3}$$

where the latter is equivalent to the Bernoulli equation. Notice that it may be shown that, suitably transformed, (3.3) includes the effect of the entrainment of momentum from the core into the turbulent region.

In (3.2) the fact is utilized that although there is a strong surface turbulence there is no external force at the free surface. It is intended that details of the analysis of flow near the free surface will be presented in a further paper. It should be emphasized, however, that this does not imply that the horizontal shear stress at $z = d$ (of which A in (2.7) is a measure) is zero. Hence the value of A is still open for discussion.

The fourth equation to be satisfied is the energy equation for the mean flow, which becomes

$$\frac{\partial}{\partial x}\int_0^d \bar{u}(g(d-z)+\tfrac{1}{2}\bar{u}^2)\,dz=\int_a^d \overline{u'w'}\frac{\partial \bar{u}}{\partial z}\,dz, \tag{3.4}$$

where the last term represents the loss of mean-flow energy due to production of turbulence. The evaluation of the right-hand side will be discussed in §4.

As mentioned in §1 the turbulence spreads downwards from the surface until the turbulent region covers the full depth. Downstream of that point we have $a = 0$, which reduces the problem to the three unknowns u_s, u_0 and d, and (3.3) is no longer valid.

By integration of (3.1), (3.2) and (3.3) with respect to x and introduction of the velocity profile (2.8), the equations transform into simple algebraic equations in the three unknowns u_s, u_0 and a. The equations can then be solved in terms of the fourth unknown d for a given value of A. Before doing so we notice that this is possible without choosing the turbulent closure, because the shear stresses in the fluid do not occur explicitly in the two momentum equations, but only in the energy equation (3.4). Hence solution of (3.4) will eventually yield the relation between d and x (i.e. $d = d(x)$).

Solution of (3.1), (3.2) *and* (3.3)

If we define the dimensionless mean velocity V as

$$V\equiv\frac{\int_0^d \bar{u}(z)\,dz}{u_0 d} \tag{3.5}$$

the continuity equation (3.1) may (after integration with respect to x) be written

$$V=(\zeta v_0)^{-1}, \tag{3.6}$$

where

$$v_0\equiv\frac{u_0}{u_1}, \quad \zeta\equiv\frac{d}{d_1}. \tag{3.7}$$

Similarly (3.3) becomes

$$v_0^2=1+\frac{2}{F_1^2}(1-\zeta) \tag{3.8}$$

with F_1 defined by (1.1), and for (3.2) we get

$$\alpha = \zeta[1+\frac{1}{2F_1^2}(1-\zeta^2)], \tag{3.9}$$

where

$$\alpha \equiv \frac{1}{d}\int_0^d \left(\frac{\bar{u}}{U}\right)^2 dz, \quad U \equiv \frac{1}{d}\int_0^d \bar{u}\, dz. \tag{3.10a, b}$$

Using (2.8) in (3.5) and (3.10) yields

$$V = 1+\Gamma\frac{b}{d}S_1 = 1+\tilde{b}S_1, \tag{3.11}$$

$$\alpha = [1+\tilde{b}(2S_1+S_2\Gamma)]\, V^{-2}, \tag{3.12}$$

where

$$S_1 \equiv \int_0^1 f(\sigma)\, d\sigma = \tfrac{1}{12}(A+4), \tag{3.13}$$

$$S_2 \equiv \int_0^1 f^2(\sigma)\, d\sigma = \tfrac{1}{105}(A^2+7A+21). \tag{3.14}$$

The procedure of solution is then: for chosen d and F_1 we get ζ from (3.7), v_0 from (3.8), and V from (3.6). Then use (3.9) to get α and determine $\tilde{b}$ and Γ from (3.11) and (3.12) respectively. Finally the three dimensional unknowns u_0, u_s and b are determined from (3.7), (2.6) and (3.11) respectively as

$$u_0 = u_1 v_0, \quad u_s = u_0(1+\Gamma), \quad b = \frac{d}{\Gamma}\tilde{b}, \tag{3.15}$$

where, in addition to F_1, we must specify either d_1 or u_1. These solutions then yield a, b, u_0 and u_s for any properly chosen d (i.e. $d_1 < d < d_2$), and hence also the velocity profile $u(z)$ for the specified depth. But no information is so far available about the relation between d and x. To obtain that part of the solution we must solve the energy equation (3.4), which again requires specification of the turbulent closure.

4. The turbulent closure

The turbulent-closure mechanism, being empirical anyway, is chosen to be as simple as possible without sacrificing the important features of the flow.

One aspect that is considered significant is associated with the fact that the bore turbulence is generated, convected (downstream), and essentially dissipated within a limited region of a few times the length of the roller. Hence, near the front where the turbulence starts there must be an excess of turbulence production relative to the dissipation, whereas further downstream the dissipation of turbulent energy ϵ must have exceeded the production.

This pattern is quite clearly illustrated if we compare the variation of the production and the dissipation from the measurements by Rouse *et al.* (1958). This is shown in figure 3.

To model this feature at least qualitatively correctly means to allow for non-equilibrium in the turbulent kinetic energy, which is defined as

$$k = \tfrac{1}{2}(\overline{u'^2}+\overline{v'^2}+\overline{w'^2}). \tag{4.0}$$

On the other hand it is considered reasonable to assume local equilibrium in the turbulent shear stresses $\overline{u'w'}$, since from a given non-equilibrium condition the various turbulent quantities relax towards local equilibrium at various rates when

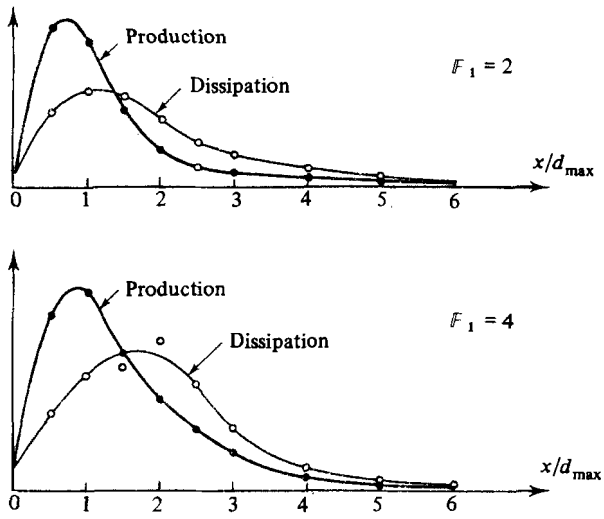

FIGURE 3. The variation with x of the depth-integrated production and dissipation of turbulent kinetic energy k, based on measurements by Rouse *et al.* (1958).

given the opportunity. And the shear Reynolds stresses are known to relax faster than either of the normal stresses and k. This implies (see Launder & Spalding 1972) that we write

$$\overline{u'w'} \propto \frac{k^2}{\epsilon}\frac{\partial \bar{u}}{\partial z}, \tag{4.1}$$

which is equivalent to using a closure model of the Boussinesq type with

$$\nu_t \propto \frac{k^2}{\epsilon}, \quad -\overline{u'w'} = \nu_t \frac{\partial \bar{u}}{\partial z}. \tag{4.2}$$

Launder & Spalding (1972) also suggest that ϵ in addition to k depends on a mixing length, which we will choose here as $d-a$. Hence we introduce for ϵ

$$\epsilon \propto \frac{k^{\frac{3}{2}}}{d-a}, \tag{4.3}$$

which in (4.2) yields

$$\nu_t \propto k^{\frac{1}{2}}(d-a). \tag{4.4}$$

By these assumptions we have reduced the turbulent-closure problem to the problem of determining k.

To do so we consider the transport equation for k, which (invoking the previous assumptions) may be written

$$\frac{dk}{dt} = \Omega_i \frac{\partial}{\partial z}\left\{\frac{k^2}{\epsilon}\frac{\partial k}{\partial z}\right\} - \overline{u'w'}\frac{\partial \bar{u}}{\partial z} - \epsilon. \tag{4.5}$$

Here and in the following all Ωs are empirical turbulent constants (see Launder & Spalding 1972).

Equation (4.5) is then integrated vertically over the turbulent region. In appendix B are shown the details of the derivation, which yields

$$\frac{\partial}{\partial x}\int_a^d \bar{u}k\,dz = \int_a^d -\overline{u'w'}\frac{\partial \bar{u}}{\partial z}dz - \int_a^d \epsilon\,dz. \tag{4.6}$$

Here the first term on the right-hand side represents the production of turbulent kinetic energy, the last the dissipation. Thus non-equilibrium for k corresponds to

$$\Lambda^2(x) \equiv \frac{\int_a^d \epsilon\, dz}{\int_a^d -\overline{u'w'}\frac{\partial \bar{u}}{\partial z}\, dz} \quad \begin{cases} < 1 & \text{near the front,} \\ > 1 & \text{further downstream.} \end{cases} \tag{4.7}$$

In harmony with (2.4) we now assume a similarity profile for k of the form

$$k^{\frac{1}{2}} = X(x)\, g(\sigma), \tag{4.8}$$

which substituted into (4.7) together with (4.2)–(4.4) and (2.7) yields that the x-variation of k must have the form

$$X(x) \propto (u_0 - u_s)\,\Lambda \left[\frac{\int_0^1 g(\sigma) f'^2(\sigma)\, d\sigma}{\int_0^1 g(\sigma)^3\, d\sigma} \right]^{\frac{1}{2}}, \tag{4.9}$$

where the bracket is a constant for specified $g(\sigma)$, and where $u_0 - u_s > 0$.

For $\Lambda = 1$ (local equilibrium in k) the model reduces to a Prandtl mixing-length theory in which

$$k^{\frac{1}{2}} \sim (d-a)\left|\frac{\partial u}{\partial z}\right| \sim f'(\sigma)\,(u_0 - u_s). \tag{4.10}$$

Hence it is natural to use $g(\sigma) = f'(\sigma)$, which then yields

$$k^{\frac{1}{2}} = \Omega_k^{\frac{1}{2}} \Lambda (u_0 - u_s) f'(\sigma), \tag{4.11}$$

and from (4.4) and (4.2) we also get

$$\nu_t = \Omega_\tau \Lambda (u_0 - u_s)\,(d-a) f'(\sigma), \tag{4.12}$$

$$-\overline{u'w'} = -\Omega_\tau \Lambda (u_0 - u_s)^2 f'^2(\sigma), \tag{4.13}$$

$$\int_a^d -\overline{u'w'}\frac{\partial \bar{u}}{\partial z}\, dz = \Omega_\tau S_{10} \Lambda (u_0 - u_s)^3, \tag{4.14}$$

where

$$S_{10} = \int_0^1 f'^3\, d\sigma. \tag{4.15}$$

The turbulence model thus introduced is a simplified k-ϵ model in which we may either determine $\Lambda(x)$ from (4.6) or use the empirical information illustrated in figure 3 to specify a reasonable algebraic closure for Λ. This is discussed further in §5.

By the derivations above we are also able to justify the form (2.7) chosen for $f(\sigma)$ by comparing the z-variation for $\bar{u}$, k and $\overline{u'w'}$ with measured values, and at the same time to discuss proper values for A.

Such a comparison is shown in figures 4–6. The measurements are taken from Rouse *et al.* (1958), Battjes & Sakai (1981), and a few from our own measurements to be described below. In figure 5 it is assumed that $\overline{u'^2} \propto k$ so that these two have the same z-variation.

In essence, the coefficient A represents $\partial u/\partial z$ at the free surface, since

$$f'(1) = 2 - A.$$

In particular $A = 2$ corresponds to $\partial u/\partial z = 0$ at the (mean) free surface, which is the usual assumption in free-surface flows, corresponding to vanishing shear stresses

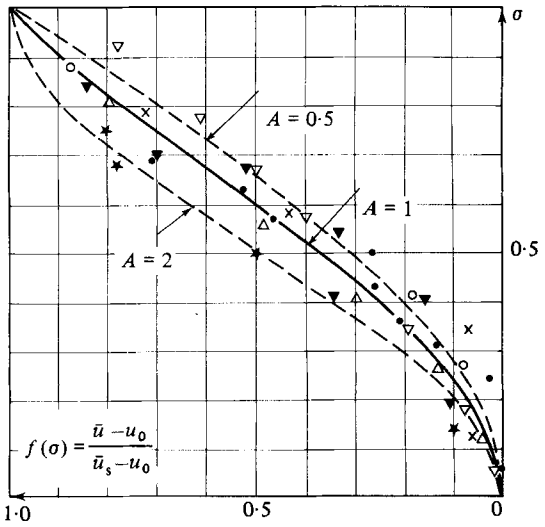

FIGURE 4. Measurements of $\bar{u}$. Rouse *et al.* (1958) ($F_1^2 = 4$: ▽, $d/d_1 = 1{\cdot}75$; △, 2·10; ○, 2·25). Own measurements ($F_1^2 = 3{\cdot}87$): ★. Battjes & Sakai (1981): ●, $x = 0{\cdot}60$ m; ×, 0·90 m; ▼, 1·20 m, +, 1·60 m.

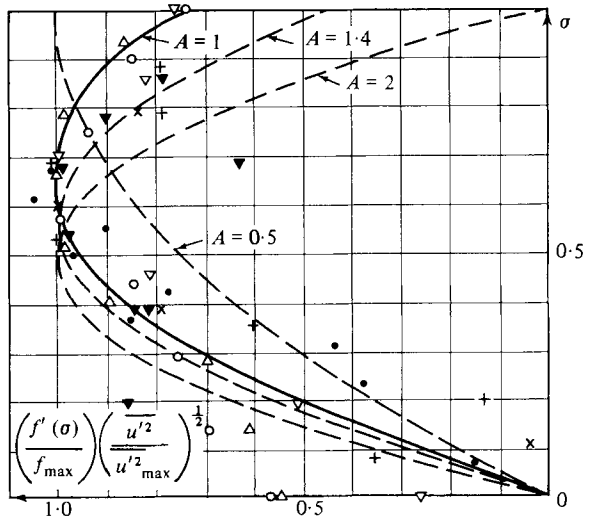

FIGURE 5. Measurements of $(\overline{u'^2})^{\frac{1}{2}}$. For symbols see figure 4.

there. $A = 2$ corresponds to the profile used by Tsubaki (1950) above $z = d_1$. Madsen & Svendsen (1979), however, showed that in the highly turbulent region of the surface roller the shear stresses will be non-zero at the local mean water level $d(x)$. So to model this effect we must choose $A < 2$. Accordingly, in the three figures we have shown curves that result from applying $A = \frac{1}{2}$, 1, 1·4 and 2.

When drawing conclusions from the figures, however, it should be recalled that the only measurements available near the surface (namely Rouse *et al.* 1958) were taken in air flow in which the 'surface' was represented by a solid wall shaped after measurements in a real hydraulic jump of the same strength. Hence by definition $\overline{u'^2}$ must be zero at $\sigma = 1$ (which means that the non-zero measurements shown for $\overline{u'^2}$

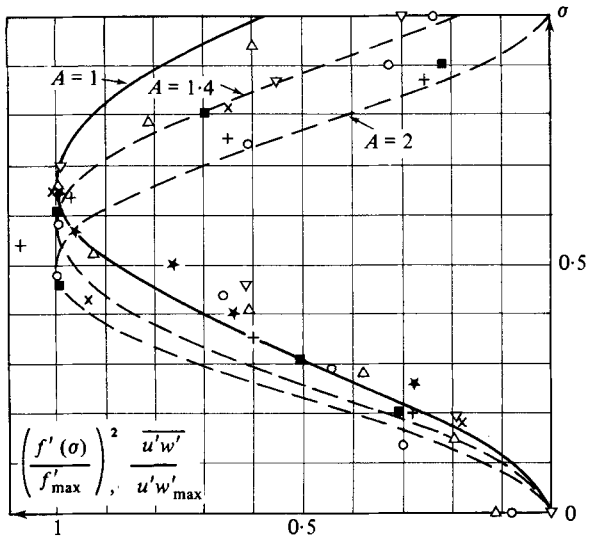

FIGURE 6. Measurements of $\overline{u'w'}$. Battjes & Sakai (1981): □, $x = 2{\cdot}00$ m. For other symbols see figure 4.

correspond to σ slightly less than 1). Therefore the measurements of Rouse *et al.* are not really relevant near the (free) surface. The measurements from Battjes & Sakai (1981) clearly show that downstream of the roller ($x > 0{\cdot}9$ m) $\overline{u'w'}$ nearly vanishes at the free surface as in ordinary free-surface flow.

In the roller Battjes & Sakai have no actual measurements near the surface, but those available clearly indicate a finite surface value for $\overline{u'w'}$. To illustrate the effect of different values of A, we will in the following give results for $A = 1$, 1·4 and 2, where these differ appreciably.

5. The surface profile

The surface profile of the jump may be found by solving the energy equation (3.4) for the mean flow. At the same time $\Lambda(x)$ must be determined, in principle from the equation (4.6) for the turbulent kinetic energy.

We first substitute (2.8) into (3.4) and define the coefficient β by

$$\beta \equiv \frac{1}{d}\int_0^d \left(\frac{\bar{u}}{U}\right)^3 dz = [1 + \tilde{b}(3S_1 + 3\Gamma S_2 + \Gamma^2 S_3)]\, V^{-3}, \tag{5.1}$$

where U is given by (3.10*b*) and

$$S_3 \equiv \int_0^1 f^3(\sigma)\, d\sigma = \tfrac{1}{840}(A^3 + 10A^2 + 45A + 120). \tag{5.2}$$

Then (3.4) becomes

$$\frac{\partial}{\partial x}[gd^2U + \tfrac{1}{2}dU^3\beta] = \int_a^d \overline{u'w'}\frac{\partial \bar{u}}{\partial z}\, dz. \tag{5.3}$$

With U eliminated by means of the continuity equation, and ζ introduced from (3.7), (5.3) may be written

$$\zeta_X\left(\frac{1}{F_1^2} - \frac{\beta}{\zeta^3}\right) + \frac{1}{2\zeta^2}\beta_X = -P_k, \tag{5.4}$$

where we have changed to

$$X = x/d_1 \tag{5.5}$$

and defined

$$P_k = \frac{1}{u_1^3}\int_0^d -\overline{u'w'}\frac{\partial \bar{u}}{\partial z}dz. \tag{5.6}$$

In a hydraulic jump ζ is a monotonic function of x, and, since from (5.1) β is a function of ζ and F_1 only, we may write

$$\beta_x = \zeta_x \frac{d\beta}{d\zeta}, \tag{5.7}$$

Substituting (5.7) into (5.4), that equation may be written

$$\zeta_X = P_k/F, \tag{5.8a}$$

where

$$F = \frac{\beta}{\zeta^3} - \frac{1}{2\zeta^2}\frac{d\beta}{d\zeta} - \frac{1}{F_1^2}, \tag{5.8b}$$

which is a first-order ordinary differential equation for $\zeta = \zeta(x/d_1)$.

From (4.14) we see that P_k is proportional to $\Lambda(x)$. In appendix C it is shown that a simple algebraic closure for Λ yields results for the surface profile that differ only slightly from the result obtained by solving the equation (4.6) for the turbulent kinetic energy.

Hence we have chosen to use the algebraic closure from appendix C:

$$\Lambda = \frac{u_0}{u_0 - u_s}, \tag{5.9}$$

and the results shown in the following are obtained with (5.9).

Notice that (5.9) satisfies the primary requirement that near the front the production of turbulent energy dominates ($\Lambda < 1$), whereas further downstream the dissipation is larger.

Figure 7 shows a comparison of the production and dissipation of turbulent energy from (5.9) with the measurements of Rouse *et al.* Considering the uncertainties of the measurements and the fact that the flow investigated by Rouse *et al.* was not a real hydraulic jump or bore, the agreement must be considered adequate.

The introduction of (5.9) for Λ also implies that only one turbulence constant Ω_τ is required, which essentially means determining the production of k at one point. This is done by comparing theoretical and measured surface profiles, and the simplest form for the equations are obtained if we consider values at the toe ($x = 0$) of the turbulent front.

It may be shown that for $x \to 0$ we get

$$\Gamma \underset{x\to 0}{\to} \Gamma_0 = -\frac{S_1}{S_2} \Leftrightarrow u_0 - u_s \to \frac{S_1}{S_2}u_0, \tag{5.10}$$

and since (5.9) implies $\Lambda = -\Gamma^{-1}$ we also have

$$\Lambda \underset{x\to 0}{\to} \Lambda_0 = \frac{S_2}{S_1}. \tag{5.11}$$

Using this together with (4.14) in (5.6), and recalling that $u_0 \to u_1$ for $x \to 0$ we find

$$P_k \underset{x\to 0}{\to} P_{k0} = \Omega_\tau S_{10}\frac{S_1^2}{S_2^2}, \tag{5.12}$$

with S_{10} given by (4.15).

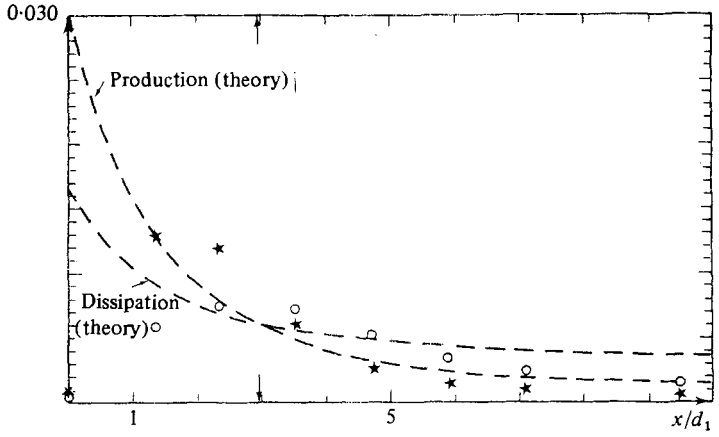

FIGURE 7. Comparison of production and dissipation of turbulence with measurements of Rouse *et al.* (1958): ★, production; ○, dissipation.

Comparison with measurements then shows the best agreement if $P_{k0} = 0{\cdot}03$, whence

$$\Omega_\tau = 0{\cdot}03 \frac{S_2^2}{S_{10} S_1^2}. \tag{5.13}$$

It is useful to compare this result with similar results for jets and mixing layers. Equation (5.13) corresponds to

$$\frac{|-\overline{u'w'}|_{\max}}{(u_0 - u_s)^2} = \begin{cases} 0{\cdot}024\Lambda & (A = 2), \\ 0{\cdot}020\Lambda & (A = 1{\cdot}4), \\ 0{\cdot}017\Lambda & (A = 1). \end{cases}$$

From Rajaratnam (1976) we find the following experimental results:

$$\frac{|-\overline{u'w'}|_{\max}}{(\Delta\bar{u})^2} = \begin{cases} 0{\cdot}023 & \text{free plane jet}, \\ 0{\cdot}018 & \text{free circular jet}, \\ 0{\cdot}026 & \text{compound jet}, \\ 0{\cdot}009 & \text{plane mixing layer}, \\ 0{\cdot}011 & \text{compound mixing layer}, \end{cases}$$

where Δu represents the maximum velocity deficit corresponding to $u_0 - u_s$. We see that for $\Lambda \approx 1$ (which is true in a large part of the flow region) (5.14) is in good agreement with the results from other types of shear turbulence.

The profiles were determined by a numerical integration of (5.8) using (5.13) for Ω_τ. With the algebraic closure used for k, Ω_τ is the only empirical constant required.

6. Comparison with measurements

The theoretical surface profiles are compared with measurements in figures 8 and 9 for $F_1^2 \approx 3{\cdot}9$ and $8{\cdot}55$ respectively. For $F_1^2 \approx 3{\cdot}9$ three different investigators have measured the surface elevations, and we see there are some discrepancies between their results.

The points denoted 'own measurements' were obtained in a 15 cm wide flume in a steady hydraulic jump generated downstream of a sluice gate (which implies that the inflow was 'undeveloped'). The measurements were taken with a resistance transducer consisting of two gold-covered silver wires with diameter 0·17 mm and

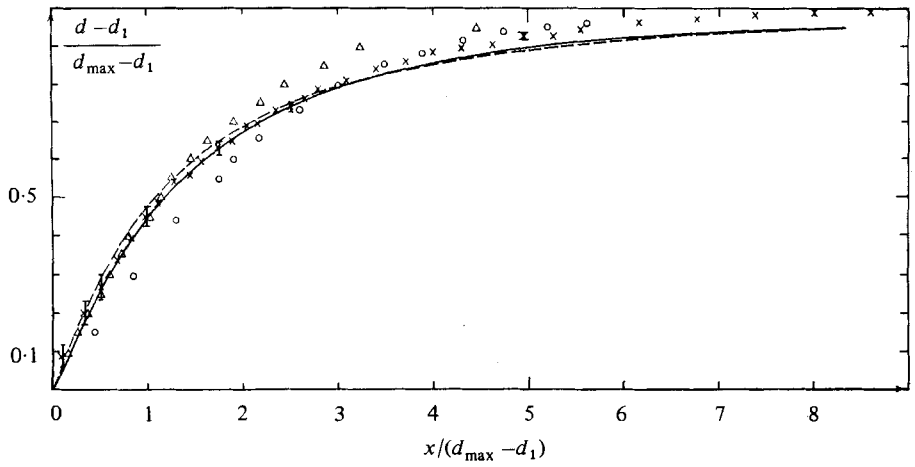

FIGURE 8. The surface profile for $F_1^2 \approx 3{\cdot}9$: △, Bakhmeteff & Matzke (1936) ($F_1^2 = 3{\cdot}94$); ○, Rouse *et al.* (1958) ($F_1^2 = 4$); ×, own measurements ($F_1^2 = 3{\cdot}87$). Bars on ×-points indicate extreme range of mean surface elevation over the 4–6 min measuring period. – – –, theory with $A = 1{\cdot}4$ ($F_1^2 = 3{\cdot}95$); ——, theory with $A = 1{\cdot}0$ ($F_1^2 = 3{\cdot}95$).

placed 5 mm apart. The electric signal was filtered to reduce the turbulent fluctuations, and measurements were taken over several minutes. The distance to the front of the jump was measured for each position of the transducer as the position of the jump was slightly sensitive to the disturbance represented by the transducer.

We see that the curves corresponding to $A = 1$ and 1·4 respectively are hardly distinguishable, although $A = 1$ does yield a slightly closer fit to the measurement in the roller region, which is in accordance with the discussion about the value of A in §4. This also confirms the expectation that the x-variations should be rather insensitive to variations in the prescribed velocity profiles.

As will be seen from (5.8) the rate of increase in the surface elevation is proportional to the local energy dissipation. Therefore when we observe that the theoretical profile is slightly lower than the measured profile in the downstream end of the jump this indicates that in that region the theoretical mean energy dissipation is a little smaller than in the experiment. The deviation is of the same order of magnitude as the 4% caused by the accumulating effect of the bottom shear stresses (see §2) which were neglected in the theory. For $F_1^2 = 8{\cdot}55$ (figure 9) we only have Bakhmeteff's data. The deviation here is slightly larger, but this should be considered in connection with the observation that for $F_1^2 \approx 3{\cdot}9$ (figure 8) where Bakhmeteff's measurements can be compared with other sources, they tend to be somewhat on the high side.

In the experiments mentioned above measurements were also taken of the mean velocity in a large number of points. A 5 mm 3-bladed micropropeller was used for this purpose, and again the results were obtained as the mean over several minutes. As the propeller cannot measure in air-entrained water, the scale of the experiment was kept small enough to prevent significant air-entrainment in the roller. (Hence the measurements also form an experimental verification, if needed, of the fact that the turbulence in a hydraulic jump can exist without air entrainment.)

In figure 10 the results of the measurements are compared with the theoretical solution described above. It has been checked that these results within the experimental accuracy satisfy the continuity equation for each velocity profile.

A single value of the mean surface velocity in the roller has also been included.

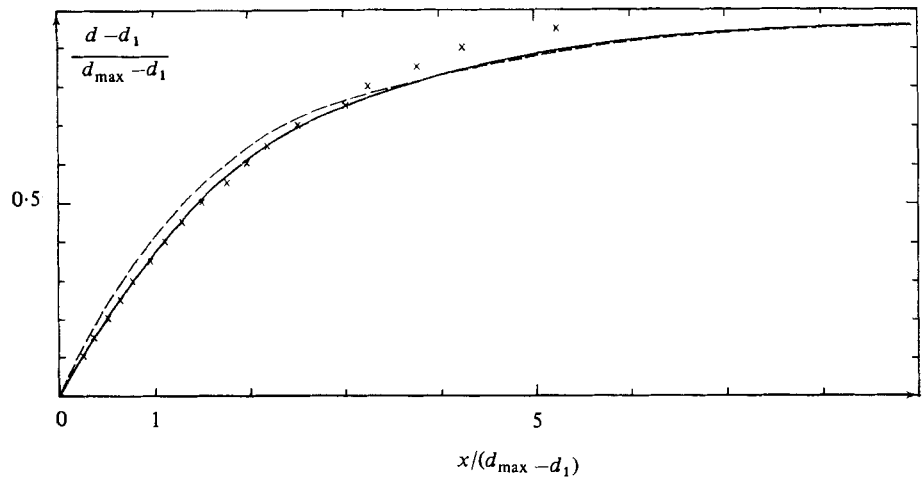

FIGURE 9. The surface profile for $F_1^2 = 8{\cdot}85$; ×, Bakhmeteff & Matzke (1936) ($F_1^2 = 8{\cdot}55$); ---, theory with $A = 1{\cdot}4$; ——, theory with $A = 1{\cdot}0$.

It was obtained by measuring on small flamingo foam particles floating on the surface. We see that within the accuracy of the measurements the general tendency in the theoretical velocity profiles is quite well confirmed.

We also notice that the difference between the profiles corresponding to $A = 1$ and 2 respectively is actually negligible in the downstream region simply because $\Gamma(x)$ in (2.8) is so small there. This confirms the decision to choose A to fit the roller profiles.

The theoretical results have also been compared with the measurements of Rouse *et al.* (1958) (figure 11) and those of Resch & Leutheusser (1972*b*) (figure 12).

As mentioned previously the experiments of Rouse *et al.* were made in a wind tunnel with the free surface simulated by a solid wall. The resulting flow is actually a diffuser in which the shear force should change sign at the (free-surface) wall, and (in particular the vertical) turbulent velocity fluctuations will vanish there.

Thus the flow especially near the free surface is significantly different from that in a bore or hydraulic jump, and therefore we cannot expect the shear stress and velocity measurements to be representative, in that region. From figure 11 this seems to apply particularly to the velocities.

Figures 11 and 12 both show significantly larger deviations for the velocity profiles than was found in our own measurements. Some of the cases (e.g. figure 12*a*), however, may be due to errors in the measurements. On the other hand, the basic idea of a turbulent layer spreading from the surface is quite clearly confirmed.

It must also be concluded that the value of A cannot be determined from the experimental results available, at least not with any further confidence than was obtained from the discussion in §4.

The measurements in figure 10 also justify the initial assumption to neglect the effect on the flow field of the bottom boundary layer. We see that the hydraulic jump behind a sluice gate shows no significant boundary layer in front of the jump (figure 10, $\delta = (d-d_1)/(d_{max}-d_1) = 0$) and even far downstream the boundary layer has not really developed yet.

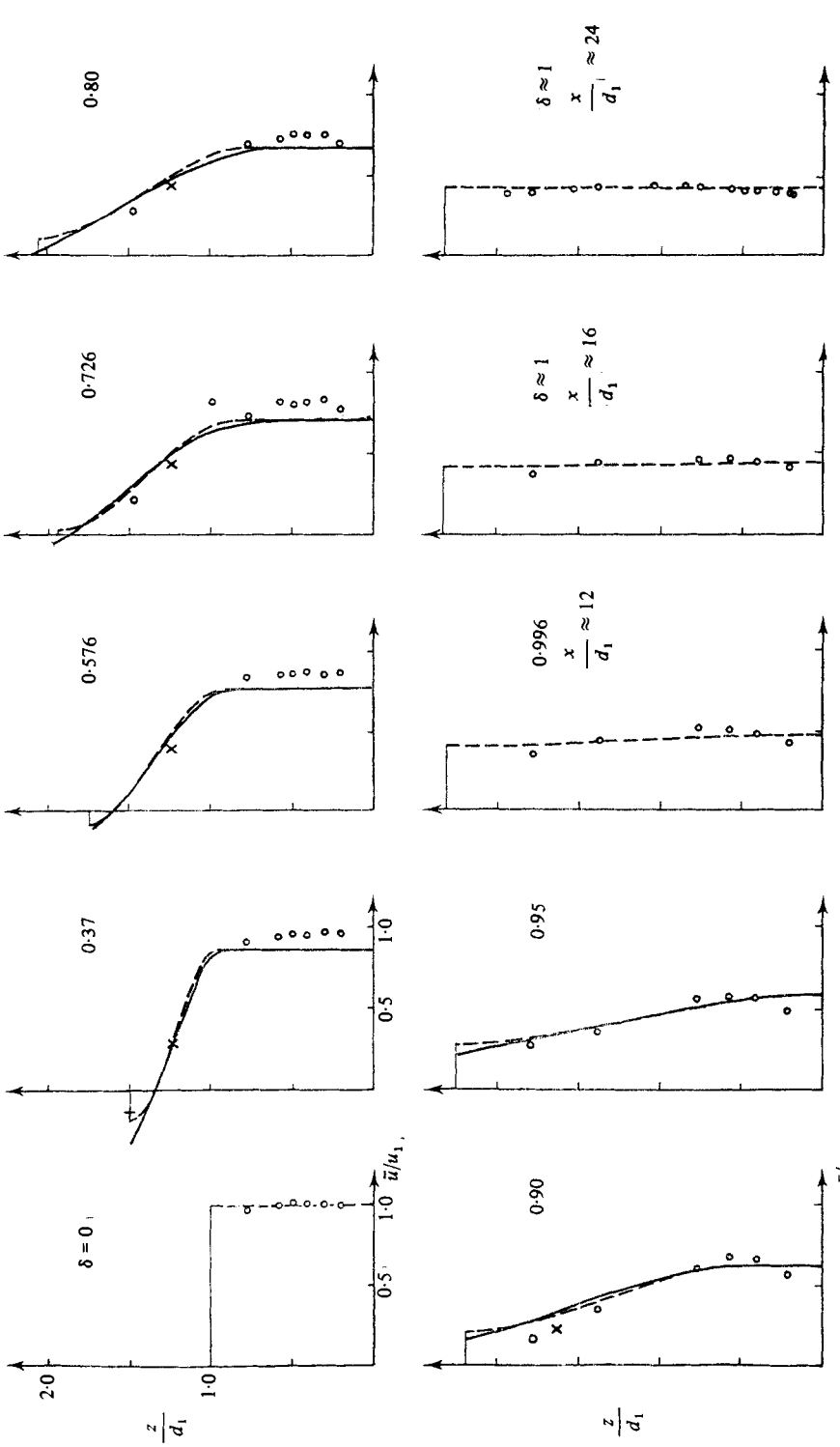

FIGURE 10. Comparison of theoretical velocity profiles with own measurements. – – –, $A = 2$; ——, $A = 1$; $F_1^2 = 3{\cdot}87$. $\delta = (d - d_1)/(d_{\max} - d_1)$.

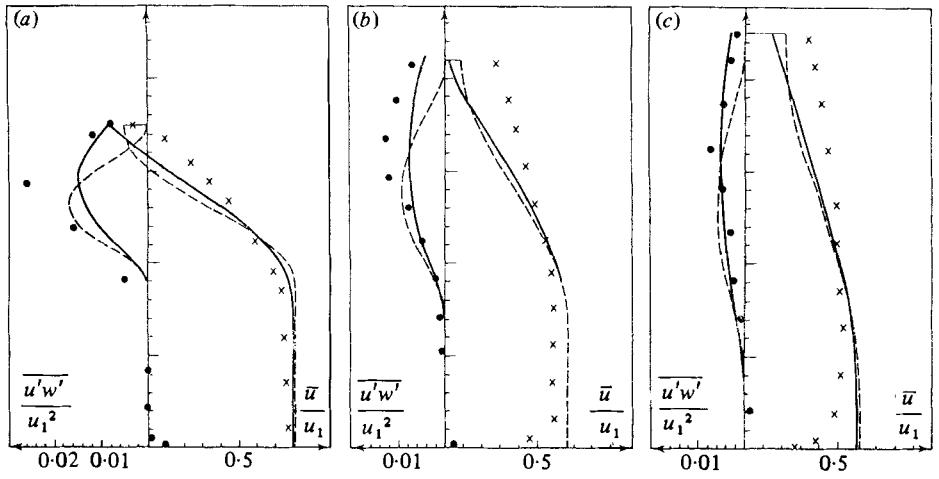

FIGURE 11. Comparison with measurements by Rouse *et al.* (1958) ($F_1^2 = 4$). ---, $A = 2$; ——, 1. (*a*) $d/d_1 = 1{\cdot}75$; (*b*) 2·10; (*c*) 2·25.

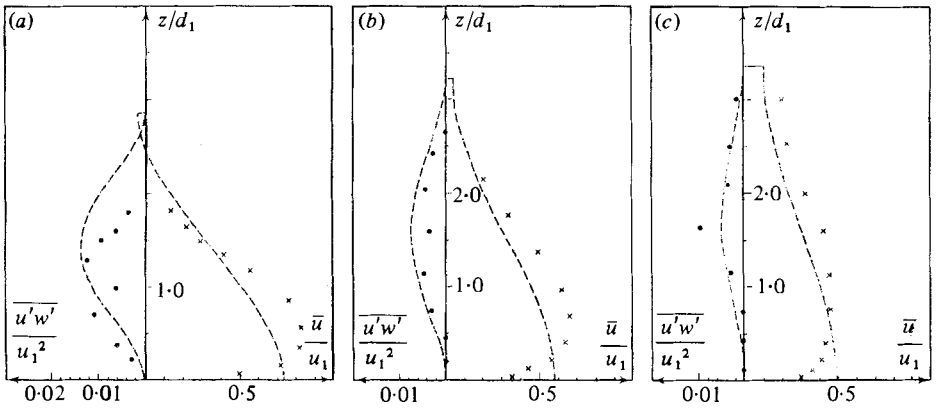

FIGURE 12. Comparison with measurements by Resch & Leutheusser (1972*b*) ($F_1^2 = 8{\cdot}12$). ---, $A = 2$. (*a*) $x/d_1 = 7{\cdot}1$; (*b*) 12·5; (*c*) 17·8.

7. Discussion of some characteristic flow details

The theoretical model developed above will predict many of the characteristic details in a bore or hydraulic jump, some of them more realistic than others.

First of all the streamline pattern may of course be derived from the solution. An example is shown in figure 13 for $F^2 = 2$. Notice that the dividing streamline separating the region of recirculation (the roller) does not coincide with the limit of the turbulent region. This limit is not even a streamline as there is a significant entrainment into the turbulent region.

What cannot really be seen is that there is a slight discontinuity in the slope of the streamlines right under the toe of the turbulent front. This is discussed further below.

In figure 14 is shown the variation of the lower limit of the turbulent region (described by a – see figure 2) for different Froude numbers. One of the interesting details is that for small Froude numbers a is increasing immediately after the start

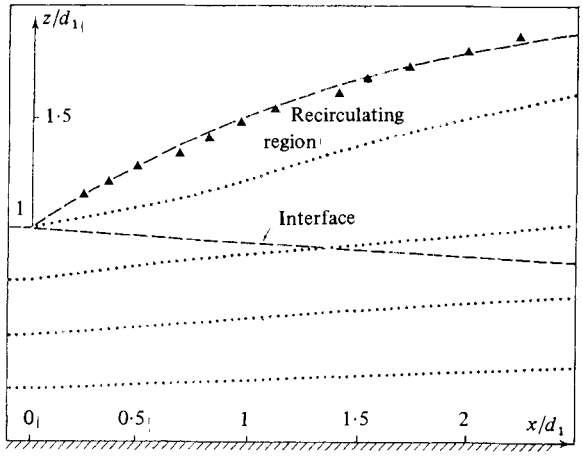

FIGURE 13. The streamline pattern in a bore/jump with $F_1 = 2$; $A = 2$. ▲, Measurements by Bakhmeteff & Matzke (1936).

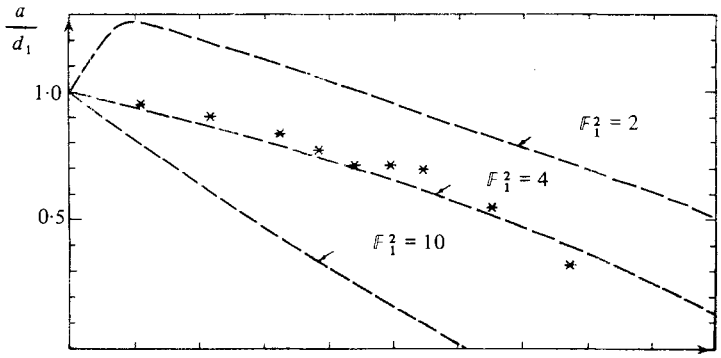

FIGURE 14. Streamwise variation of the distance from the bottom to the lower limit of the turbulent region.

of turbulence, which means that although the turbulence is spreading downwards from the surface the slope of the surface is larger. This situation may be recognized in some of the photographs in Peregrine & Svendsen (1978). The larger the Froude number the steeper the increase in the turbulent region.

The effect of the turbulence in preventing the bore front from gradually steepening as it propagates (as it would in the nonlinear shallow-water theory with static pressure and a depth-independent velocity profile) is expressed by the way the total horizontal momentum is conserved at any point in the jump. The equation describing this is (3.9), which shows that to obtain momentum balance at any point (with the permanent form assumed in that equation) the velocity profile must deviate from the z-independent profile in such as way that α varies as prescribed by that equation. This requires a transfer of momentum upwards from the lower layers in the jump and this is exactly what the turbulence causes. Figure 15 shows the α-variation required according to (3.9).

Hence we must imagine the interaction between the turbulence and the shape of the bore or jump is such that if the front is too steep the surface water will rush faster down the slope to create more-violent turbulence as it meets the incoming water at

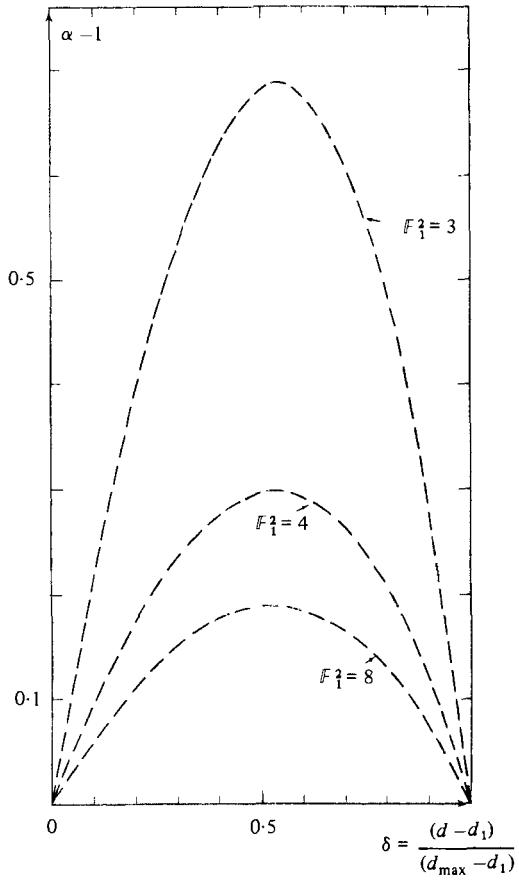

FIGURE 15. The variation of α according to (3.9).

the toe. In the theory described above this is heuristically modelled by using Λ proportional to the difference $u_s - u_0$ between surface and bottom velocities. The details, however, of how a deviation from the stable profile is stabilized by the turbulence cannot be analysed in the present formulation of the theory, which assumes permanent form. It will be discussed in a later paper.

It is worth mentioning another feature of the theoretical model associated with the flow around the front. In the model the flow upstream of the toe cannot feel the coming front. In this sense the model is a shock model, which is of course not in accordance with the assumption of incompressible potential flow outside the turbulence region. In reality, the pressure change represented by the front will be felt also upstream of the toe, which can also be seen from the abovementioned photographs, where a weak rise in the water level occurs in front of the turbulent bore with a similar slight change in the streamlines. It is the omission of this effect that causes the abovementioned discontinuity in the slope of the streamlines.

Other, but physically more reasonable, discontinuities occur at the front. Thus the surface velocity u_s is finite even at the toe. This is not in conflict with continuity, as the thickness of the layer (the 'roller') with this property tends to zero as $x \to 0^+$. Figure 16 shows this property in terms of Γ, which is part of the solution. The value of Γ at $x = 0^+$ is given by (5.10) and also the value of other quantities may be

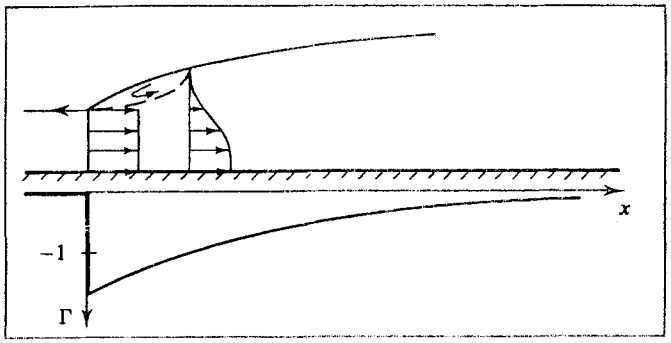

FIGURE 16. The variation of the surface velocity represented by $\Gamma = (u_s - u_0)/u_0$.

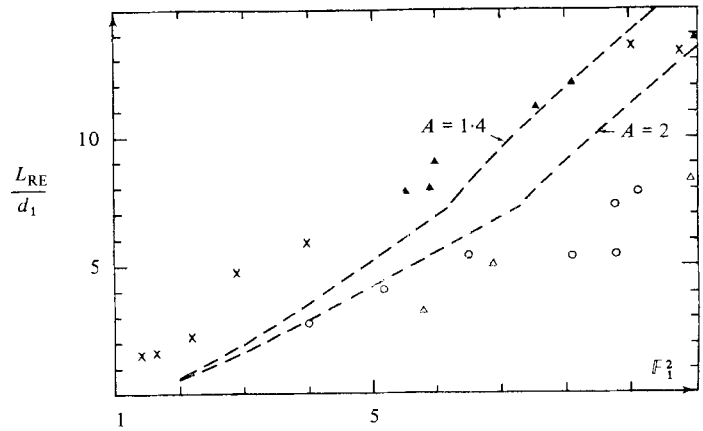

FIGURE 17. Length L_{RE} of the roller as a function of F_1.

determined at the toe. Of particular interest is that the surface slope ζ_x is given by

$$\zeta_x = 2\Omega_r S_{10} \frac{S_1^2}{S_1 S_3 - S_2^2} \frac{F_1^2}{F_1^2 - 1} \quad (x = 0^+), \tag{7.1}$$

which shows that the bore or jump is steeper the smaller the Froude number F_1.

Finally the 'length of the roller' L_{RE} may of course be determined from the results as the value of x for which $u_s = 0$. But, as one physically feels that this quantity is very sensitive to small changes in the flow pattern, so the computations show that it depends quite strongly on the value of A. As figure 17 shows, measurements of L_{RE} confirm this transitoriness.

8. Summary and conclusions

The model developed for bores and hydraulic jumps is based on satisfying the hydrodynamic equations 'at large' by considering the equations integrated over the depth (or part of the depth). This is combined with an assumption of static pressure, which is shown to be well justified (see appendix A), and with a specification of the vertical variation of the velocity profile (2.8) and (2.7). A qualitative illustration of the flow pattern is shown in figure 2.

In the turbulent region a closure model is used which allows non-equilibium in the

turbulent kinetic energy k. The final closure used for k is algebraic (implying that only one empirical constant Ω_τ describes the turbulence), but in appendices B and C the depth-integrated transport equation for k is derived and solved to show that little is gained by this more elaborate procedure.

Finally the results for both the surface profile and the velocity and shear-stress variations are compared with measurements.

A number of conclusions may be drawn from the analysis and the comparisons.

It is shown by varying the prescribed velocity profile (by changing the constant A) that the surface profile is insensitive to the precise form of the velocity profile. There is good agreement with measurements for rather different A-values.

On the other hand, the comparison with, in particular, our own measurements shows that the prescribed vertical variation of the velocities is in good agreement with measurements.

Yet insufficient information is available about both velocities and shear stresses near the surface where the flow is dominated by gravity and the high-intensity surface turbulence. Hence there is a need for measurements in that region.

The bottom boundary layer and shear stresses have been neglected, which is natural in a bore and is shown by the measurements to be a good approximation for a jump behind a sluice gate. By restricting the analysis to such flows we also avoid the problem of separation of the bottom boundary layer due to the adverse pressure gradient under the jump (or even formation of a standing vortex near the bottom), which may occur in cases of a 'fully developed' inflow.

Finally it may be added that since the flow far downstream of the jump or bore returns to the steady uniform free-surface flow both the total height of the jump and the total power dissipation are determined by the classical formulas known from the hydraulic textbooks.

Appendix A

The deviation from static pressure will change the total momentum in any vertical section. In this appendix it is shown that the change is negligible.

The total momentum, assuming a static pressure distribution, is

$$M_S = \alpha\rho U^2 d + \tfrac{1}{2}\rho g d^2, \tag{A 1}$$

where α is defined by (3.10).

In fact, the pressure is non-hydrostatic. The pressure is given by (see e.g. Madsen & Svendsen 1979)

$$p(z) = \rho g(d-z) - \rho w^2 + \frac{\partial}{\partial x}\int_z^d \rho uw\,dz + \text{terms from the surface turbulence.} \tag{A 2}$$

At the bottom we have $p \equiv p_b$ and $w = 0$, so that

$$p_b = \rho g d + \frac{\partial}{\partial x}\int_0^d \rho uw\,dz. \tag{A 3}$$

Rajaratnam (1965) finds experimentally for all x that $p_b \approx \rho g d$, so that we must have $(\partial/\partial x)\int_0^d \rho uw\,dz = 0$. Now $\bar{u}$ and $\bar{w}$ have the same sign at all points, so since $\partial/\partial x$ of vertical turbulent shear stress $\int \overline{u'w'}\,dz$ is negligible we have

$$\frac{\partial}{\partial x}\int_z^d \rho uw\,dz \approx \frac{\partial}{\partial x}\int_z^d \rho\bar{u}\bar{w}\,dz = 0. \tag{A 4}$$

Hence (A 2) becomes

$$p(z) \approx \rho g(d-z) - \rho w^2 \tag{A 5}$$

or

$$\frac{p(z)}{p_b} \approx \frac{d-z}{d} - \frac{w^2}{gd}, \tag{A 6}$$

which shows that the deviation from static pressure is represented by w^2/gd. Rajaratnam (1965) finds that for a jump with $F_1 = 2{\cdot}86$ the maximum deviation from static pressure is $\approx 0{\cdot}1 p_b$. Part of this contribution is due to $\overline{w}^2$, the rest (near the surface particularly) is caused by the turbulent fluctuations $\overline{w'^2}$. Therefore we get corresponding to (A 1) for non-hydrostatic pressure

$$M = \rho g d^2 \left(\alpha \frac{U^2}{gd} + \frac{1}{2} - \int_0^d \frac{w^2}{gd} dz \right). \tag{A 7}$$

If, inspired by Rajaratnam's (1965) graph, we assume (for the $F_1 = 2{\cdot}86$) jump

$$\int_0^d \frac{w^2}{gd} dz \approx 0{\cdot}6 \times 0{\cdot}1 = 0{\cdot}06$$

we get

$$\frac{M}{M_S} = \frac{\alpha F^2 + \frac{1}{2} - 0{\cdot}06}{\alpha F^2 + \frac{1}{2}},$$

where $F^2 \equiv U^2/gd$ varies streamwise between $F_1^2 > 1$ in the front of the jump and $F_2^2 < 1$ downstream of the jump. Since $w^2/gd \approx 0{\cdot}1$ is a maximum value occurring under the roller it is natural to combine this with $F \approx 1$, which yields (with $\alpha \approx 1{\cdot}4$, see figure 15)

$$\frac{M}{M_S} = 0{\cdot}968,$$

i.e. the deviation from static pressure contributes at most 3·2 % to the total momentum, or about 1·6 % to the depth.

Finally we notice that since w/U varies only slightly with the strength of the jump we must have $w^2/gd \propto F^2$ so that the above analysis holds at least for a wide range of jumps.

Thus we conclude that the deviation from the static pressure will have very little effect on the momentum balance.

Appendix B

Equation (4.6) is found by integrating (4.5) over the turbulent region. This yields, since the flow is steady, for the term on the left-hand side

$$\int_a^d \frac{dk}{dt} dz = \int_a^d \left(\bar{u} \frac{\partial k}{\partial x} + \bar{w} \frac{\partial k}{\partial z} \right) dz = \int_a^d \frac{\partial}{\partial x} (\bar{u}k)\, dz + [\bar{w}k]_{z=d}, \tag{B 1}$$

the latter being obtained by means of the continuity equation and $k = 0$ at $z = a$. The Leibnitz rule then gives

$$\int_a^d \frac{dk}{dt} dz = \frac{\partial}{\partial x} \int_a^d \bar{u}k\, dz - [\bar{u}k\eta_x + \bar{w}k]_{z=d} = \frac{\partial}{\partial x} \int_a^d \bar{u}k\, dz, \tag{B 2}$$

where the kinematic free-surface condition

$$\bar{w} - \bar{u}\,\bar{\eta}_x = 0 \tag{B 3}$$

has been invoked.

For the first term on the right-hand side of (4.5) we get directly

$$\int_a^d \frac{\partial}{\partial z}\left(k^{\frac{1}{2}}(d-a)\frac{\partial k}{\partial z}\right)dz = k^{\frac{1}{2}}(d-a)\frac{\partial k}{\partial z}\Big|_a^d, \tag{B 4}$$

where $k = 0$ at $z = a$. The value of the result at $z = d$ represents the net diffusion of k through the mean free surface due to the turbulent surface fluctuations. Since only a small fraction of the energy dissipation occurs above $z = d$ this contribution is negligible. Hence we arrive at the depth-integrated transport equation

$$\frac{\partial}{\partial x}\int_a^d \bar{u}k\,dz = -\int_a^d \overline{u'w'}\frac{\partial \bar{u}}{\partial z}dz - \int_a^d \epsilon\,dz, \tag{B 5}$$

which is (4.6). This also implies that the value of Ω_i in (4.5) becomes irrelevant.

Appendix C. Solution of the transport equation for k

The depth-integrated transport equation for k (4.6) may be transformed into a differential equation for Λ^2 (defined by (4.7)) by the following operations.

First we eliminate P_k defined by (5.6) between (4.6) and (5.8) and get

$$\frac{\partial}{\partial x}\int_a^d \bar{u}k\,dz = (1-\Lambda^2)\,u_1^3 F\zeta_x d_1. \tag{C 1}$$

We then transform to ζ as independent variable (see the comments in §5) to obtain

$$\frac{\partial}{\partial \zeta}\int_a^d \bar{u}k\,dz = (1-\Lambda^2)\,u_1^3 F d_1. \tag{C 2}$$

Substituting (2.4) and (4.11) for u and k then yields

$$\Omega_k F_1 \frac{d\Lambda^2}{d\zeta} + \Lambda^2(\Omega_k F_2 + F) - F = 0, \tag{C 3a}$$

$$F_1 = \frac{1}{u_1^3 d_1}[(u_0-u_s)^2 b(u_0 S_{11} - (u_0-u_s)S_{12})], \tag{C 3b}$$

$$F_2 = dF_1/d\zeta, \tag{C 3c}$$

$$S_{11} \equiv \int_0^1 f'^2(\sigma)\,d\sigma = \tfrac{1}{15}(2A^2-5A+20), \tag{C 3d}$$

$$S_{12} \equiv \int_0^1 f(\sigma)f'^2(\sigma)\,d\sigma = \tfrac{1}{120}(A^3+8A^2-32A+96). \tag{C 3e}$$

Equation (C 3a) is the required equation for Λ^2. F_1 and F_2 are functions of the other variables u_0, u_s and b. Hence the inclusion of this equation means that the model consists of the algebraic equations in §3 plus the two simultaneous differential equations (5.8) and (C 3a).

The inclusion of (C 3) requires an (extra) boundary condition for Λ, and it is natural to specify the value of Λ at the toe of the jump, i.e. $\zeta = 1$. Here one would expect both dissipation and production of turbulent energy to grow with the size of the turbulent region so that their ratio Λ may have a limiting value for $\zeta \to 1$, which could be used as the boundary condition for (C 3a).

It turns out, however, that $F_1 \underset{\zeta\to 1}{\to} 0$ so that (C 3a) is singular at $\zeta = 1$. The inner

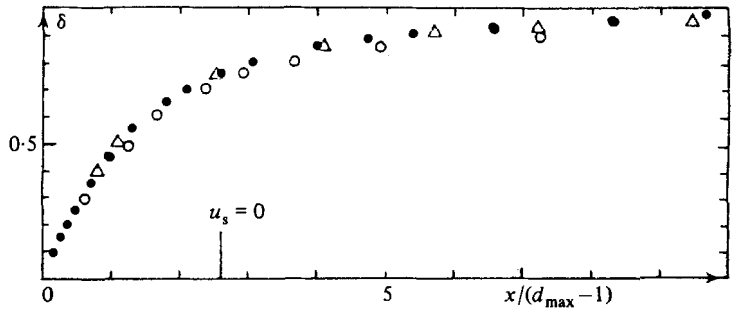

FIGURE 18. Comparison between solution with algebraic closure (C 7) and with transport equation (C 3). $F_1^2 = 4$, $A = 1{\cdot}4$, Ω_r from (5.13). ●: $\Lambda = u_0/(u_0 - u_s)$; △, transport equation for Λ, $\Omega_k = 0{\cdot}0754$; ○, transport equation for Λ, $\Omega_k = 0{\cdot}01$.

approximation of (C 3a) valid for small $\xi = \zeta - 1$ may be written

$$\frac{d\Lambda^2}{d\xi} + \frac{\Lambda^2}{\xi} C_1 = \frac{C_2}{\xi}, \tag{C 4a}$$

where

$$C_1 = (F_2 + C_2)_{\zeta=1}, \quad C_2 = \left(\frac{F}{\Omega_k}\right)_{\zeta=1}, \tag{C 4b}$$

which has the complete solution

$$\Lambda^2 = \frac{C_2}{C_1} + C\xi^{-C_1} \quad (\zeta \to 1). \tag{C 5}$$

Hence if we wish to keep Λ^2 bounded for $\zeta \to 1$ we must use $C = 0$ (since $C_1 > 0$), which corresponds to $d\Lambda^2/d\xi \to 0$ for $\zeta \to 1$, and (C 5) becomes

$$\Lambda_{\zeta\to 1} = \left(\frac{F}{\Omega_k F_2 + F}\right)_{\zeta=1}^{\frac{1}{2}} = \left[1 - 2\Omega_k \frac{S_1 S_2 - S_2 S_{11}}{S_1 S_3 - S_2^2}\right]^{-\frac{1}{2}}. \tag{C 6}$$

The value of $\Lambda_{\zeta\to 1}$ cannot be deduced from the measurements available, but if (C 6) is going to equal the value of the algebraic closure

$$\Lambda = \frac{u_0}{u_0 - u_s} \tag{C 7}$$

at $\zeta \to 1$ then we must have $\Omega_k = 0{\cdot}0754$. It may be shown that this value is slightly larger than the value in jets and mixing layers, where we find $0{\cdot}015 < \Omega_k < 0{\cdot}055$, and also larger than the value of $0{\cdot}022 < \Omega_k < 0{\cdot}044$, which can be derived from the experiments of Rouse *et al.* (1958).

Figure 18, however, shows a comparison between the surface profiles obtained by using (C 7), and (C 3a) with the boundary condition (C 6) respectively. For the latter case is shown the result for two rather different values of Ω_k (0·01 and 0·0754), and we conclude that the solution using (C 7) is as accurate as the more elaborate differential closure described by the transport equation for k, which in itself is not very sensitive to the value of Ω_k.

REFERENCES

ABRAMOVICH, G. N. 1963 *The Theory of Turbulent Jets.* MIT Press.

BAKHMETEFF, B. A. & MATZKE, A. E. 1936 The hydraulic jump in terms of dynamic similarity. *Trans. ASCE* **101**, 630–647.

BATTJES, J. A. & SAKAI, T. 1981 Velocity fields in a steady breaker. *J. Fluid Mech.* **111**, 421–437.

BÉLANGER, J. M. 1828 *Essai sur la Solution Numérique de Quelques Problèmes, Relatives au Mouvement Permanent des Eaux Courantes.* Paris.

FALKNER, V. M. & SCAN, S. W. 1930 Some approximate solutions of the boundary layer equations. *ARC R. & M.* no. 1314.

FINLAYSON, B. A. 1972 The method of weighted residuals and variational principles. *Maths in Sci. and Engng* **87**.

HARLEMAN, D. R. F. 1958 Discussion on Rouse *et al.* (1958). *J. Hydraul. Div. ASCE* **84** (HY6), 1856-52–55.

HIBBERD, S. & PEREGRINE, D. H. 1979 Surf and run-up on a beach: a uniform bore. *J. Fluid Mech.* **95**, 323–345.

JOHNS, B. 1980 The modelling of the approach of bores to a shoreline. *Coastal Engng* **3**, 207–219.

KÁRMÁN, T. VON 1930 Mechanische Ähnlichkeit und Turbulenz. *Nachr. Ges. Wiss. Göttingen, Math. Phys. Kl.*

KELLER, H. B., LEVINE, D. A. & WHITHAM, G. B. 1969 Motion of a bore over a sloping beach. *J. Fluid Mech.* **7**, 302–316.

LAUNDER, B. E. & SPALDING, D. B. 1972 *Mathematical Models of Turbulence.* Academic.

LONGUET-HIGGINS, M. S. & TURNER, J. S. 1974 An entraining plume model of a spilling breaker. *J. Fluid Mech.* **63**, 1–20.

MADSEN, P. A. 1981 A model for a turbulent bore. *Series Paper* 28, *Inst. Hydrodyn. and Hydraul. Engng, Tech. Univ. Denmark.*

MADSEN, P. A. & SVENDSEN, I. A. 1979 On the form of the integrated conservation equations for waves in the surf zone. *Prog. Rep.* 48, *Inst. Hydrodyn. and Hydraul. Engng, Tech. Univ. Denmark*, 31–39.

MAVIS, F. T. & LUKSCH, A. 1936 Discussion of Bakhmeteff & Matzke (1936). *Trans. ASCE* **101**, 669–672.

NARAYANAN, R. 1975 Wall jet analogy to hydraulic jump. *J. Hydraul. Div. ASCE* **101** (HY3), 347–359.

PEREGRINE, D. H. 1972 Equations for water waves and the approximations behind them. In *Waves on Beaches* (ed. R. E. Meyer). Academic.

PEREGRINE, D. H. 1974 Water wave interaction in the surf zone. In *Proc. 14th Conf. on Coastal Engng*, pp. 500–517.

PEREGRINE, D. H. & SVENDSEN, I. A. 1978 Spilling breakers, bores, and hydraulic jumps. In *Proc. 16th Coastal Engng Conf.*, chap. 30, pp. 540–550.

RAJARATNAM, N. 1965 The hydraulic jump as a wall jet. *J. Hydraul. Div. ASCE* **91** (HY5), 107–131.

RAJARATNAM, N. 1967 Hydraulic jumps. *Adv. Hydrosci.* **4**, 197–280.

RAJARATNAM, N. 1976 *Turbulent Jets.* Elsevier.

RESCH, F. J. & LEUTHEUSSER, H. J. 1972*a* Reynold stress measurements in hydraulic jumps. *J. Hydraul. Res.* **10**, 409–430.

RESCH, F. J. & LEUTHEUSSER, H. J. 1972*b* Le ressaut hydraulique; mesure de turbulence dans la région diaphasique. *Houille Blanche* **4**, 279–293.

RESCH, F. J., LEUTHEUSSER, H. J. & COANTIC, M. 1976 Étude de la structure cinématique et dynamique du ressaut hydraulique. *J. Hydraul. Res.* **14**, 293–319.

ROUSE, H., SIAO, T. T. & NAGARATNAM, S. 1958 Turbulence characteristics of the hydraulic jump. *J. Hydraul. Div. ASCE* **84** (HY1), 1528-1–30.

SARMA, K. V. N. & NEWHAM, D. A. 1973 Surface profiles of hydraulic jump for Froude numbers less than four. *Water Power* **25**, 139–142.

SVENDSEN, I. A. & JONSSON, I. G. 1976 Hydrodynamics of coastal regions. *Den Private Ingeniørfond, Tech. Univ. Denmark.*

SVENDSEN, I. A., MADSEN, P. A. & BUHR HANSEN, J. 1978 Wave characteristics in the surf zone. In *Proc. 16th Coastal Engng Conf., Hamburg*, chap. 29, pp. 520–539.

TSUBAKI, T. 1950 Theory of hydraulic jump. *Rep. Res. Inst. for Fluid Engng, Kyushu Univ., Fukuoka, Japan* **6**, 2.